


RESEARCH ARTICLE | APRIL 19 2017

Time-resolved image plane off-axis digital holography

N. V. Petrov ; S. E. Putilin; A. A. Chipegin



Appl. Phys. Lett. 110, 161107 (2017)

<https://doi.org/10.1063/1.4981899>



 **Hall Effect Measurement Handbook** 

A comprehensive resource for both new and experienced material researchers

Hall Effect Measurement Handbook
A Fundamental Tool for Semiconductor Material Characterization
Jeffrey Lindemuth, PhD
Edited by David C. Povey

Time-resolved image plane off-axis digital holography

N. V. Petrov,^{a)} S. E. Putilin, and A. A. Chipegin

Department of Photonics and Optical Information Technology, ITMO University, Kronverkskiy prospekt, 49, St. Petersburg 197101, Russia

(Received 8 February 2017; accepted 9 April 2017; published online 19 April 2017)

In this work, we demonstrate off-axis image-plane digital holography for measuring ultrafast processes with high temporal resolution. The proposed image-plane holographic configuration in conjunction with numerical post-processing procedures allows us to neglect the walk-off effect in the off-axis arrangement by synthesizing spatial phase distribution with the whole field of view from separate fragments and to increase the spatial resolution by means of a telecentric system with adjustable magnification. We have analyzed temporal resolution taking into account all dispersing elements that increase the duration of the pulses being propagated through the optical setup. The technique was approved with experiment on measuring the dynamics of the refractive index, induced by laser filamentation in air. *Published by AIP Publishing.*

[<http://dx.doi.org/10.1063/1.4981899>]

Time-resolved digital holography is a promising technique for application in various spheres of science and technology because it allows diagnosing and investigating ultrafast processes.

The key feature of time-resolved digital holography is the ability to measure the spatial distribution of the phase delay with ultra-high temporal resolution, and therefore, temporal dynamics of processes and phenomena of various characteristics can be investigated. For instance, it allows obtaining quantitative information on refractive index variation of the medium as a result of the spark discharge at high voltage,¹ making possible the analysis of ultrafast laser damage processes in thin films.² The use of reflection and transmission interferometers allows us to study surface deformation and refractive index change simultaneously.³

Other examples include investigations of spatial and temporal interactions during self-focusing of ultrashort light pulses, accompanied by plasma filamentation.^{4–7}

During the last decade, various configurations of time-resolved digital holography were proposed. The inline scheme is easier to build because the hologram is created with one beam.^{4,5} The main drawback of the inline arrangement is that the reconstructed object, conjugate image, and zero order term are aligned. Techniques that use iterative algorithms allow accurate reconstruction of the inline holograms^{8,9} but require additional processing power. The demonstrated femtosecond pulsed phase-shifting layout requires a micro-polarizer array conjugated with an image sensor.¹ The off-axis scheme⁶ prevents the superposition of real and twin images with the zero order term and can be built with simple experimental facilities, but the walk-off effect takes place in this case. The interference field, where pulses overlap in space, decreases linearly with their duration due to the group velocity mismatch limiting the coherence zone. Balčūnas *et al.*⁷ exclude the problem by organizing the interference from tilted wavefronts that have angular chirp.

However, that technique requires considering the group dispersion delays at the object and reference arms; otherwise, the relative position of the spectral components in the arms will be different, leading to the degradation of the hologram and causing low temporal resolution. Another method applicable for recurrent processes is associated with synthesizing holograms with the whole field of view through the stitching of the set of subholograms,¹⁰ obtained by scanning the optical delay line in the reference arm. The disadvantages of this method are related to the procedure of synthesizing the full field of view hologram. Aberrations of the subholograms, caused by, e.g., mechanical vibrations, air disturbance, and translational errors of the delay line, will degrade the quality of the reconstructed image.

In this work, we propose Time-Resolved Image Plane Off-axis Digital Holography (TRIPODH), which allows us to eliminate the walk-off problem due to transferring the synthesizing full field of view image procedure to the last step of the reconstruction algorithm where the resulting phase images are obtained.

The proposed method works in conjunction with the local least-squares wave retrieval algorithm.¹¹ The method does not require back propagation and gives high contrast at the edges in virtue of careful interferometric processing. The image is retrieved directly from image plane interferogram.¹² The proposed image plane schematics provides the following advantages: (i) there is no need for the numerical simulation of the wavefront back-propagation from the object plane to the registration plane; (ii) $4f$ optical system transfers the image from the object plane to the registration plane and allows adjusting the magnification coefficient depending on the required field of view and the spatial resolution. The last is not limited by the pixel size, compared to the Fresnel configuration. Just changing the ratio between focal lengths of the lenses in our system provides a possibility to investigate objects of microscopic and macroscopic scales; (iii) telecentric configuration is an efficient solution for physical compensation of spherical aberrations in digital holographic microscopy.^{13,14}

^{a)} Author to whom correspondence should be addressed. Electronic mail: n.petrov@niuitmo.ru

The TRIPODH experimental setup is based on a laser system producing femtosecond pulses with dozens of field oscillation (Fig. 1). The beam from the laser system is split on the pump beam and two beams for holographic imaging: object and reference. The delay line controls the reference beam, which allows us to manage the position of the reference beam in space at a time. The latter affects the position of the interferometric fringes relatively to the image of the object. Thus, we are able to scan the image of the object (Fig. 1), which has been transferred to the registration plane, where a recording camera is placed. The transfer of the image is reached through the optical elements depending on the desired magnification.

The temporal resolution in such a system is limited by the duration of the pump pulse. As the pulse propagates, it suffers the dispersive broadening on the elements of the optical system.^{15,16} The duration of the broadened pulse can be estimated from Equation (1)

$$\hat{\tau} = \tau \sqrt{1 + \frac{\left[(\Delta l_{BS} + \Delta l_{lens}) \left(\frac{\lambda^3}{2\pi c^2} \frac{\partial^2 n}{\partial \lambda^2} \right) \right]^2}{16ln^2(2)\tau^4}}, \quad (1)$$

where τ is the full width at half maximum duration of the initial pulse, $\Delta l_{BS} + \Delta l_{lens}$ is the length of the optical elements, λ is the wavelength, n is the refractive index, and c is the speed of light.

Temporal resolution of the method is limited by duration of the pulse in the object arm before the moment when the pulse interacts with the object. Using formula (1), we can estimate that transparent moving objects, e.g., filaments, with the transverse size of less than $100 \mu\text{m}$, do not make a perceptible contribution in temporal broadening of the object beam with intensity, which does not exceed 10^8 W/cm^2 . In

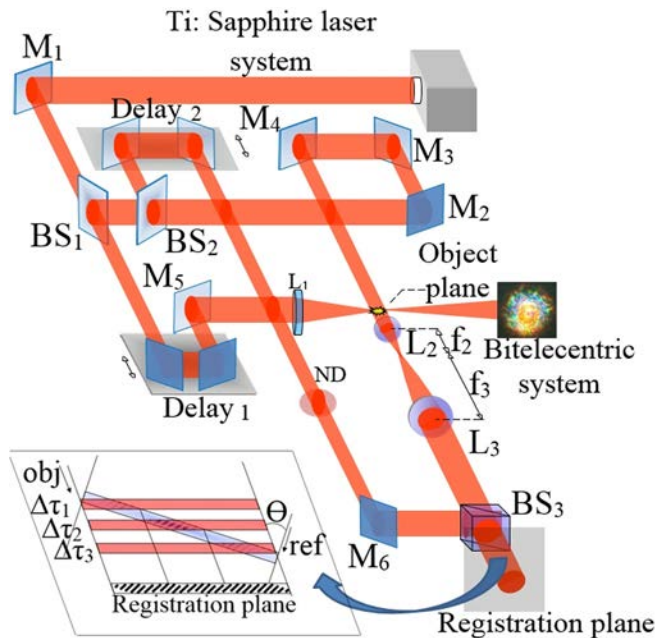


FIG. 1. TRIPODH experimental setup. BS₁, BS₂, and BS₃ are beam splitters; M₁-M₆ are mirrors; ND is the neutral density filter; L₁-L₃ are lenses; Delay₁ and Delay₂ are mirror delay lines of the object and reference beams, respectively.

such a case, the temporal broadening of the object pulse is linear and depends mainly on the refractive index of the object, which does not exceed 10^{-3} . The contribution to the temporal broadening of the moving object is comparable with the contribution of dielectric mirrors that we used to reduce the dispersion effect. Chirped dielectric structures are effective for controlling the broadband dispersion.¹⁷ As soon as the pulse reaches the object and experiences phase shift, its duration does not affect the temporal resolution. The reference beam and object beam interfere with each other after the broadening. The interference pattern depends on the duration of the pulses and the angle between them.

In order to obtain quantitative information about the phase of the object from the recorded holograms, we perform several procedures: (i) reconstruct the phase of the subholograms, (ii) subtract the background, (iii) stitch phase of the reconstructed subholograms into a whole field of view hologram, and (iv) apply the phase matching algorithm.

- (i) For phase reconstruction, we use the complex wave retrieval algorithm, based on the local least squares estimation algorithm (LLS).
- (ii) To obtain the phase retardation, when the wavefront of the probe beam suffers from aberrations (e.g., due to inaccuracies in adjusting the optical system), we record the hologram of the background and subtract it from the hologram of the object. To provide more accurate wavefront reconstruction, advanced LLS techniques^{18,19} can be used to eliminate more efficiently the noise in the initial estimation and preserve important phase object details.
- (iii) The set of subholograms of the magnified object was recorded in order to overcome the limit on the number of fringes k , when using ultrashort pulses, that do not cover the whole object (Equation (2))

$$k = \frac{c\tau_p}{\lambda}. \quad (2)$$

The phases from the reconstructed set of the subholograms are being stitched to cover the whole object with the extended field of view. The use of the telecentric system with magnification allows making the carrier fringes extremely short, and thus, spatial resolution for off-axis digital holographic microscopy achieves the resolution of the inline configuration and phase-shifting holography as will be discussed later.

- (iv) The phase matching algorithm is applied when phases of two subholograms differ by a constant. This could happen, e.g., when the reference beam is tilted relatively to the object beam. The mismatch of the optical axis and translation stage delay₂, which controls the delay time of the beams, causes a wavefront tilt from one subhologram to another. After background subtraction using interferometric methods,²⁰ we equalize the phase retardation of the images by changing the wavefront phase for each subhologram by a constant relatively to the initial subhologram. This subroutine reduces requirements to the fine adjustment of the experimental setup.

Figure 2 represents procedures for obtaining quantitative information. Depending on the beam size, size of the object, and magnification coefficient of the optical system, we set the number of subholograms N and the window size WS in pixels. We record N subholograms of the object O^t ($O^1 \dots O^N$), and the background B^t ($B^1 \dots B^N$), where t is the index of the subhologram, which is referred to the delay time between reference and object beams. The number of subholograms, which need to be recorded, depends on the size of the object and the resolution of the imaging system. Using the LLS algorithm, we obtain phases of the object ϕ_O^t and the background ϕ_B^t . The actual values of the ϕ_O^t and ϕ_B^t will be discussed in the experimental approbation of the technique. Subtraction of the background removes the aberrations. The process of equalizing the images is reached through adding a constant C^t to each subhologram. The procedures repeat N times.

In experimental approbation of the technique, we used a Ti:Sapphire laser system (regenerative amplifier Regulus 35F1K, Avesta Project) with a central wavelength of 800 nm, a repetition rate of 1 kHz, and a 2.3 mJ energy per pulse generating 30 fs pulses for off-axis hologram generation. Laser radiation is divided into two channels by means of a beam splitter 1 (Fig. 2). A beam with 0.1 mJ energy is reserved for holographic imaging, which is limited by the sensitivity of the camera. It is important to avoid the filament generation in the Fourier plane. Neutral density (ND) filters are used for aligning the intensity of reference and object beams to obtain maximum visibility of the interfering fringes at the image plane. The remaining laser energy reflected from the beam splitter was used to form an ultrafast recurrent process, the appearance of which is controlled by delay line 1. Laser radiation was focused with L_1 with $f_1 = 10$ cm, thus generating the ultrafast process of laser filamentation at the

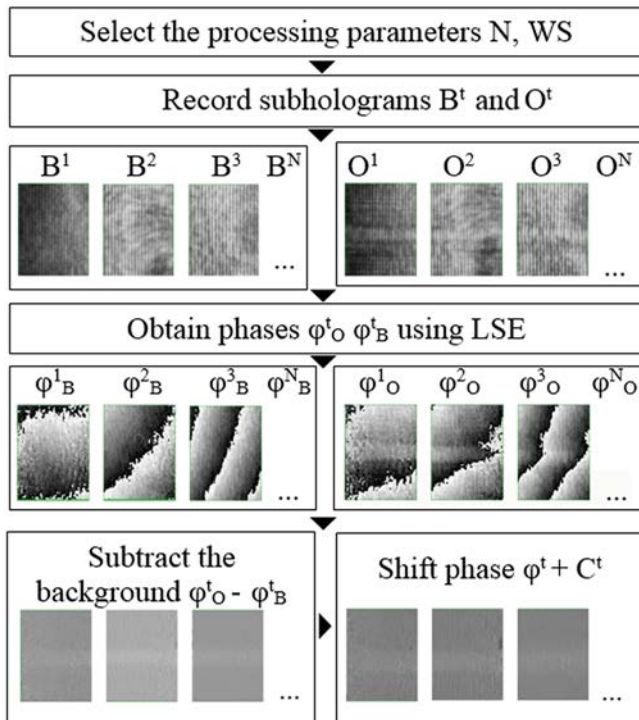


FIG. 2. Procedures for obtaining quantitative information about the phase of the object.

object plane. Time alignment of the filament's appearance and reference and object beams was carried out with two delay lines. Using beam splitter cube 3 with the size of 3 cm, reference and object beams were converged together and interfered. For registration of the interference pattern, we used a NIKON D7000 camera (CMOS matrix with pixel size of $4.7 \mu\text{m}$).²¹ The exposure time of the camera is 0.6 s, which allowed us to record and average the effect from the number of pulses that passed during this time.

The spatial resolution of the reconstructed off-axis hologram in such a system depends on the area, where pulses overlap. The size of the overlap area L is given by (3)

$$L = \frac{c\tau}{\sin \theta}. \quad (3)$$

Increasing the angle of incidence θ reduces the area, where pulses overlap, as the fringes become more dense and thinner.

The effective pixel size $\Delta\hat{x}$ in such configuration is

$$\Delta\hat{x} = \frac{\Delta x}{M}, \quad (4)$$

where Δx is the real pixel size without magnification.

To estimate the spatial resolution capabilities of the bitemcentric system, we build up two telescopes with magnifying coefficients $M = 1.5$ and $M = 6$. In the case of the $1.5\times$ telescope, the effective pixel size was estimated to be $2 \mu\text{m}$ with the fringe size of $10 \mu\text{m}$. For the $6\times$ telescope, the effective pixel size was estimated to be $0.5 \mu\text{m}$ with the fringe size of $2.5 \mu\text{m}$. The images and cross-sections of the test object¹⁸ with different resolutions are presented in Fig. 3, where red arrows and blue arrows show the cross-sections for $1.5\times$ and $6\times$ telescopes, respectively.

From Figure 3, we can see that the test object is resolved better with the $6\times$ telescope. Some sharp edges are not resolved with the $1.5\times$ telescope.

The angle between the object beam and the reference beam in our main experiment was 1.59° . Such an angle

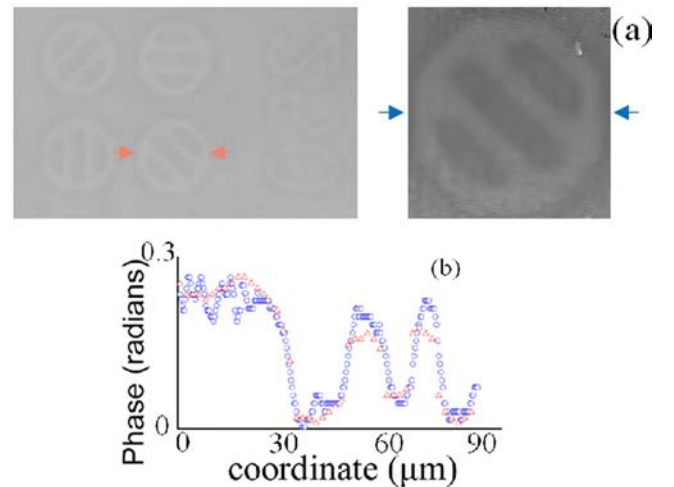


FIG. 3. Test object (a) and cross-sections (b) resolved with different magnifying systems. The image on the left, where the place of the cross-section denoted by red arrows, is made with magnifying coefficient $M = 1.5$. The image on the right is made with magnifying coefficient $M = 6$, and the cross-section is denoted by blue arrows.

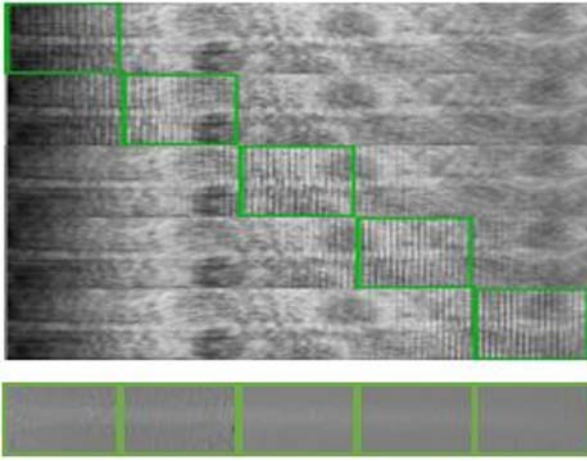


FIG. 4. 5 subholograms of the different parts of the object and phase image stitched from reconstructed phases of subholograms.

provides the size of each fringe to be 6 pixels without magnification and temporal coherence to be 80 fs, which corresponds to $24 \mu\text{m}$ for the coherence length.

To transfer the image from the object plane to the registration plane, we set up the bitemporal system that consists of two lenses. The front focus was aligned with the filament and the rear focus with the registration plane. The bitemporal system magnifies the image depending on the focal length of the lenses. By changing the delay time between the reference beam and the object beam, we managed the position of the interferometric fringes to record a set of subholograms to cover the full object (see Fig. 1: delays $\Delta\tau_1$, $\Delta\tau_2$, and $\Delta\tau_3$). Lenses with focal lengths $f_2 = 10 \text{ cm}$ and $f_3 = 3.3 \text{ cm}$ give a magnifying coefficient $M = 3$ and for each fringe 2 effective pixels $\Delta\hat{x}$ are required. Figure 4 illustrates 5 subholograms in space with respect to the object. The full field of view phase image is compiled from fragments. The step of the delay $\Delta\tau_1$ is $1 \mu\text{m}$ corresponding to 6.7 fs, which allows us to control the evolution of the filament with high temporal resolution.

Figure 5 represents reconstructed and stitched phase contrast images for various time delays (250, 500, and 750 fs) of the filament. As the filament evolves, we can see from

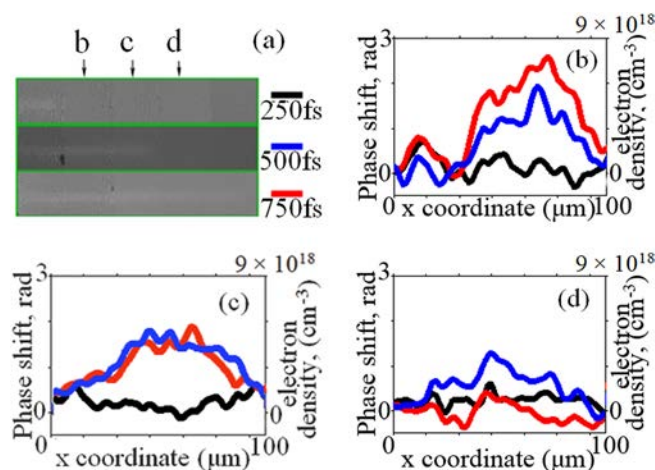


FIG. 5. Reconstructed phase of the filament evolution at 250 fs, 500 fs, and 750 fs (a) and transverse sections at different positions (b), (c), and (d).

transverse sections at different positions (b, c, and d) that the phase increases from 0.1 rad (black line 250 fs) up to 2.8 rad (red line 750 fs).

In accordance with the reconstruction method, spatial phase distributions and electron density induced by the filament for various time delays were obtained. Electron density was calculated using the formula

$$n_e = \frac{-2n_{cr}\Delta\theta\lambda}{2\pi d}, \quad (5)$$

where n_e is the electron density, n_{cr} is the critical plasma density in air, for $\lambda = 800 \text{ nm}$ $n_{cr} = 1.7 \times 10^{21} \text{ cm}^{-3}$, d is the diameter of the filament, and $\Delta\theta$ is the phase change. Maximum phase change is less than 3 rad, which corresponds to electron density of $9 \times 10^{18} \text{ cm}^{-3}$. The results of the experiments are in good agreement with similar measurements by means of an interferometric method. In Ref. 4, authors used radiation from a Ti:Sapphire laser amplifier with laser pulses of 2 mJ and 150 fs duration to create a filament with an electron density of $7.03 \times 10^{18} \text{ cm}^{-3}$. According to Ref. 22, the electron density is highly dependent on the focal length, and for 10 cm lens, the electron density is calculated to be $2 \times 10^{18} \text{ cm}^{-3}$. In Ref. 8, authors used the pump beam with only $35 \mu\text{m}$, which was focused using a 0.11 numerical aperture (NA) (10 \times) microscope objective. The use of the telecentric system allows us to resolve peaks of electron density in highly limited space. The power of the pulse does not exceed 10^8 W/cm^2 and the spectrum bandwidth remains constant, and hence, the coherence length also remains constant. Due to the constant coherence length, the interference pattern did not depend on the broadening of the probe pulse. After propagation, the lenses in the bitemporal system and beam splitter cube with 3 cm size pulse stretched in time from 30 fs up to 129.4 fs. The pulse width was approximated with Sech² shape and was calculated as

$$\tau_{\text{sech}^2} = \frac{\tau}{1.5426}. \quad (6)$$

Autocorrelation shots made with autocorrelator ASF-20 (Avesta project) of the initial pulse and the pulse at image plane are presented (Fig. 6).

As it was shown, the temporal stretch of the pulse depends on the initial duration of the pulse, propagation path, and characteristics of the media.^{23–26} The group velocity was estimated to be $2.0054 \times 10^8 \text{ m/s}$, the refractive index was 1.5108, and group velocity dispersion was $44.6820 \text{ fs}^2/\text{mm}$.

In conclusion, we have demonstrated off-axis image-plane digital holography for measuring ultrafast processes

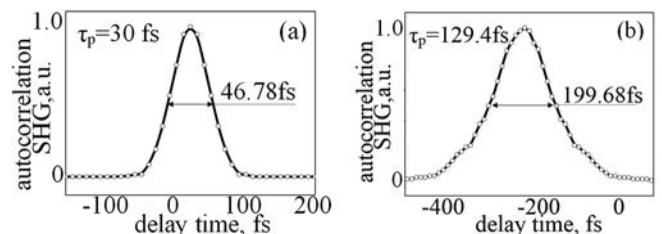


FIG. 6. Autocorrelation shots of the initial pulse (a) and the pulse propagated to the registration plane (b).

with high temporal resolution. The walk-off problem was eliminated by recording a set of subholograms and stitching the phases of the reconstructed subholograms. The bitelecentric system allows us to effectively increase the spatial resolution of the reconstructed wavefront. Among other off-axis schemes, the TRIPODH obtains one of the highest results and allows us to use contemporary methods for accurate reconstruction of the wavefront from noisy data. Temporal resolution in our method is limited only by duration of the initial pulse, before it interacts with the dynamic object, allowing us to study the dynamic processes of the femtosecond order.

This work was partially financially supported by the Ministry of Education and Science of the Russian Federation, Grant Nos. 3.1893.2017 and 3.9041.2017, Government of the Russian Federation 074-U01 and was supported by the Russian Foundation for Basic Research (RFBR), Project No. # 16-52-52049/16.

- ¹T. Kakue, S. Itoh, P. Xia, T. Tahara, Y. Awatsuji, K. Nishio, S. Ura, T. Kubota, and O. Matoba, *Opt. Express* **20**, 20286 (2012).
- ²N. Šiaulys, L. Gallais, and A. Melninkaitis, *Opt. Lett.* **39**, 2164 (2014).
- ³L. Zhu, C. Zhou, T. Wu, W. Jia, Z. Fan, Y. Ma, and G. Niu, *Appl. Opt.* **49**, 2510 (2010).
- ⁴M. Centurion, Y. Pu, Z. Liu, D. Psaltis, and T. W. Hänsch, *Opt. Lett.* **29**, 772 (2004).
- ⁵M. Centurion, Y. Pu, and D. Psaltis, *J. Appl. Phys.* **100**, 063104 (2006).
- ⁶T. Balčūnas, A. Melninkaitis, A. Vanagas, and V. Sirutkaitis, *Opt. Lett.* **33**, 58 (2008).
- ⁷T. Balčūnas, A. Melninkaitis, A. Vanagas, and V. Sirutkaitis, *Opt. Lett.* **34**, 2715 (2009).
- ⁸S. Tzortakis and D. Papazoglou, *Appl. Phys. Lett.* **93**, 041120 (2008).
- ⁹D. Abdollahpour, D. G. Papazoglou, and S. Tzortzakakis, *Phys. Rev. A* **84**, 053809 (2011).
- ¹⁰L. Zhu, M. Sun, J. Chen, Y. Yu, and C. Zhou, *Opt. Eng.* **52**, 091703 (2013).
- ¹¹M. Liebling, T. Blu, and M. Unser, *J. Opt. Soc. Am. A* **21**, 367 (2004).
- ¹²G. B. Brandt, *Appl. Opt.* **8**, 1421 (1969).
- ¹³E. Sánchez-Ortiga, P. Ferraro, M. Martínez-Corral, G. Saavedra, and A. Doblas, *J. Opt. Soc. Am. A* **28**, 1410 (2011).
- ¹⁴A. Doblas, D. Hincapie-Zuluaga, G. Saavedra, M. Martínez-Corral, and J. García-Sucerquia, *Appl. Opt.* **54**, 5229 (2015).
- ¹⁵A. Chipegin and A. Tsyppkin, in *Proceedings of the 2015 IEEE North West Russia Section Young Researchers in Electrical and Electronic Engineering Conference (EIconRusNW 2015)* (2015), p. 125.
- ¹⁶A. Tsyppkin, S. Putilin, and S. Kozlov, *Opt. Spectrosc.* **114**, 863 (2013).
- ¹⁷R. Szipöcs, C. Spielmann, F. Krausz, and K. Ferencz, *Opt. Lett.* **19**, 201 (1994).
- ¹⁸V. Katkovnik, I. A. Shevkunov, N. V. Petrov, and K. Egiazarian, *Proc. SPIE* **9508**, 950802 (2015).
- ¹⁹V. Katkovnik, I. Shevkunov, N. V. Petrov, and K. Egiazarian, *Opt. Express* **24**, 25068 (2016).
- ²⁰A. Belashov, N. Petrov, and I. Semenova, *Opt. Express* **22**(23), 28363 (2014).
- ²¹V. Lesnichii, N. Petrov, and P. Cheremkhin, *Opt. Spectrosc.* **115**, 577 (2013).
- ²²F. Théberge, W. Liu, P. T. Simard, A. Becker, and S. L. Chin, *Phys. Rev. E* **74**, 036406 (2006).
- ²³O. Martínez, R. Fork, and J. Gordon, *Opt. Lett.* **9**, 156 (1984).
- ²⁴Y. Zhang, S. Qiao, L. Sun, Q. W. Shi, W. Huang, L. Li, and Z. Yang, *Opt. Express* **22**, 11070 (2014).
- ²⁵G. Pedrini, W. Osten, and Y. Zhang, *Opt. Lett.* **30**, 833 (2005).
- ²⁶E. Escoto, J. Muldera, L. Dasallas, E. Estacio, and P. Almoró, *Opt. Commun.* **329**, 190 (2014).